Structural Differences between Aβ(1-40) Intermediate Oligomers and Fibrils Elucidated by Proteolytic Fragmentation and Hydrogen/Deuterium Exchange

Aming Zhang,[†] Wei Qi,[†] Theresa A. Good,[‡] and Erik J. Fernandez[†*]

[†]Department of Chemical Engineering, University of Virginia, Charlottesville, Virginia 22904; and [‡]Department of Chemical and Biochemical Engineering, University of Maryland Baltimore County, Baltimore, Maryland 21250

ABSTRACT The aggregation of amyloid-β protein (Aβ) in vivo is a critical pathological event in Alzheimer's disease. Although more and more evidence shows that the intermediate oligomers are the primary neurotoxic species in Alzheimer's disease, the particular structural features responsible for the toxicity of these intermediates are poorly understood. We measured the peptide level solvent accessibility of multiple Aβ(1-40) aggregated states using hydrogen exchange detected by mass spectrometry. A gradual reduction in solvent accessibility, spreading from the C-terminal region to the N-terminal region was observed with ever more aggregated states of Aβ peptide. The observed hydrogen exchange protection begins with reporter peptides 20-34 and 35-40 in low molecular weight oligomers found in fresh samples and culminates with increasing solvent protection of reporter peptide 1-16 in long time aged fibrillar species. The more solvent exposed structure of intermediate oligomers in the N-termini relative to well-developed fibrils provides a novel explanation for the structure-dependent neurotoxicity of soluble oligomers reported previously.

INTRODUCTION

Studies over the last two decades have accumulated a large body of evidence in favor of the amyloid hypothesis, which regards the cerebral Aβ accumulation as the primary driving force in Alzheimer's disease pathology (1,2). Consequently, the process of Aβ aggregation and fibril formation has been explored extensively in AD research (3–9). Two intriguing but unresolved issues are the underlying molecular mechanism by which in vivo generated Aβ peptide forms neurotoxic oligomers and fibrils, and the molecular basis for the differences in neurotoxicity associated with different aggregated forms, with an increasing emphasis on the intermediate soluble oligomers (10–13). Clear elucidation of the structural and kinetic aspects of aggregate formation is crucial to the development of therapeutic strategies to address AD.

In the process of Aβ fibrillogenesis, both the initial and final states of Aβ peptide have been well characterized by multiple biophysical methods (8,9,14). Molecular level 3D structural models of Aβ fibrils have been proposed independently by several research investigators that agreed in the fundamental parallel, in-register, cross-β assembly pattern (15–17). Conversely, the intermediate oligomers, which are increasingly thought to be the most toxic species in AD, are much less understood because of their transient, heterogeneous nature. Although classifications may vary, three distinct groups of Aβ aggregation intermediates have been identified before (7,18). Among them, low molecular weight (LMW) oligomers consist of a narrow distribution of dimers to hexamers (or somewhat larger), which are seen frequently to be equilibrated rapidly with Aβ monomer in freshly prepared samples (18,19). High molecular weight (HMW) oligomers generally refer to larger Aβ aggregates showing a 9–25 nm diameter spherical or disc-like morphology (8,10,13,20). Aβ protofibrils are defined as the smallest unit of mature fibrils, exhibiting Congo Red and thioflavin T (ThT) binding, and ordered β-sheet structure (21–23). However, a detailed molecular level structure difference between intermediate Aβ oligomers and maturely developed fibrils has not been identified. Consequently, the molecular basis for the observed structure-dependent neurotoxicity of Aβ aggregates are likewise unclear (10,24).

We have reported previously that multiple aggregated Aβ(1–40) species can be distinguished by their degree of solvent accessibility using hydrogen exchange mass spectrometry (HX-MS) without proteolysis (25). Separate peaks in HX mass spectra were assigned to a particular aggregated species using multiple techniques, including size exclusion chromatography (SEC), electron microscopy (EM), and atomic force microscopy (AFM) as described previously (13,25). We elucidate the local structural differences of Aβ(1-40) peptide formed in four increasingly aggregated states by comparing their peptide level solvent accessibility patterns measured by HX-MS. Due to the use of two different immobilized enzyme columns (pepsin and type XIII fungal protease in tandem), we increased the number of Aβ cleavage sites, thus the number of available reporter peptides, which enabled the analysis of solvent accessibility at enhanced spatial resolution (26). Most importantly, two sets of intermediate Aβ oligomers (i.e., LMW and HMW oligomers) were examined for the first time by this approach

Submitted June 9, 2008, and accepted for publication October 9, 2008.

*Correspondence: erik@virginia.edu

Editor: Heinrich Roder.

0006-3495/09/02/1091/14 $2.00

doi: 10.1016/j.bpj.2008.10.022

without the aid of any structure stabilizing agents, and they were distinguished structurally from the well-developed fibrils by their solvent accessibility patterns. We believe these results help to provide new insight in the structural basis for the distinct neurotoxicity associated with different aggregated forms of Aβ (13).

MATERIALS AND METHODS

Materials

Aβ(1-40) was obtained from AnaSpec (San Jose, CA) as vials of 1.0-mg lyophilized powder. Deuterium oxide (D_2O) was obtained from Cambridge Isotope Laboratories (99.9% Deuterium; Andover, MA). Pepsin from porcine gastric mucosa and type XIII fungal protease from *Aspergillus saitoi* were obtained from Sigma-Aldrich (St. Louis, MO). All other chemicals were purchased from Sigma unless otherwise specified.

Sample preparation

All the Aβ(1-40) samples were prepared in the same way as our previous HX-MS study of intact Aβ without proteolytic fragmentation (25). Briefly, fresh Aβ samples were made by mixing 4.3 μL stock solution (10 mg/mL in 0.1% trifluoroacetic acid (TFA; Fluka, Ronkonkoma, NY) solution) with 95.7 μL PBS buffer (10 mM NaH_2PO_4, 150 mM NaCl, pH 7.4) to a peptide concentration of 100 μM. Aged Aβ samples were prepared by quiescently incubating the same diluted Aβ solution (100 μM in PBS buffer) at 37 $\pm$ 0.5°C for desired times; we studied 4-h, 72-h, and 6-day aged samples mainly. To ensure the pattern of aggregation was reproducible, the same lot of Aβ was used for all experiments.

Deuterium labeling

Basically, the same procedure (25) was used for the deuterium labeling of most Aβ samples by directly mixing 5 μL Aβ solution with 45 μL D_2O in 1.5 ml Eppendorf centrifuge tube, giving a 90% deuterium (molar fraction) in the labeling solvent. However, the 6-day aged sample was treated somewhat differently before labeling. it was washed once to produce a relatively pure fibril sample by centrifugation at 13,000 $\times$ *g* for 10 min. Ninety microliters of supernatant was removed and replaced by the same volume of D_2O to initiate the deuterium labeling. Thirty seconds of rigorous vortexing was applied to resuspend fibrils. All the hydrogen-deuterium (H/D) exchange reactions were carried out at pH 7.0 (as read with deuterium present) and room temperature. The labeling times were chosen based on the dynamic stability of analyzed Aβ samples, and are specified in Results.

After labeling for the desired times, Aβ aggregates were dissociated back into monomeric state for mass spectrometer detection under conditions where the H/D exchange was quenched. To increase the signal/noise ratio (S/N) in acquired mass spectra, fresh, and aged Aβ samples were processed differently after the labeling step. For the fresh sample, H/D exchange reaction was quenched by adding 30 μL mixture of dimethyl sulfoxide and dichloroacetic acid (Fluka) (v/v, 95:5) to the 50 μL labeling solution to decrease pH to 3.0 (as read). For the aged samples, large Aβ aggregates (mainly HMW oligomers and fibrils) were concentrated by centrifugation at 13,000 $\times$ *g* for 10 min. After removal of the supernatant, 30 μL dimethyl sulfoxide/dichloroacetic acid mixtures were added. The effect of centrifugation operation on deuterium labeling for aged samples was shown to be negligible by comparing the labeling results of reporter peptide 20-34 (the one with highest S/N ratio, data not shown) without centrifugation step.

Enzyme digestion and HPLC procedures

The H/D exchange quenched samples were diluted to a low organic solvent concentration by adding 420 μL 0.05% formic acid (FA) in D_2O/H_2O mixture (90:10, molar ratio). The pH was maintained around 2.7 (as read). The diluted sample was immediately injected into a 200 μL stainless steel sample loop and then delivered through two immobilized enzyme columns (pepsin and fungal protease type XIII in tandem) to the C_{18} small molecule trapping column (1 mm ID $\times$ 8 mm, catalog No. TR1/25108/01; Michrom Bioresources, Auburn, CA). An isocratic stream of 5% acetonitrile (ACN) and 0.1% FA in distilled, deionized water (H_2O) was used. The flow rate was 200 μL/min. To prepare the pepsin and fungal protease type XIII columns, immobilized enzyme beads (POROS-20AL; Applied Biosystems, Sunnyvale, CA) were prepared and packed into column (2.1 mm ID $\times$ 30 mm, catalog No. 2-3008-05; Applied Biosystems) according to the manufacturer's instructions. A bed volume of ~100 μL led to ~30 s of digestion time in each enzyme column. The digested peptide mixture was desalted for 3 min, and then eluted from the trapping column using a gradient of ACN fraction from 5% to 50% over 5 min at flow rate of 50 μL/min. The two composite solvents were 0.1% FA and 0.01% TFA in ddH_2O (solvent A) and 0.2% FA in ACN (solvent B). The eluted peptide mixture was sent to mass spectrometer for analysis. To minimize artifactual exchange during the analysis time, all the columns, loops, and lines were immersed in ice bath during all the experiments.

Mass spectrometry

Mass spectra were acquired by a linear ion trap mass spectrometer with a standard electrospray ionization source (LTQ, Thermo Electron Corporation, San Jose, CA) at scanning mode of positive polarity, zoom scan, and selected ion monitoring. Eight discrete *m/z* ranges were specified to simultaneously detect the eight proteolytic reporter peptides during each run. Other acquisition parameters were set as follows: capillary temperature: 250°C, spray voltage: 4.3 kV, sheath gas flow: 40 unit, capillary voltage: 15 V; tube lens voltage: 105 V.

Spectral deconvolution and artifactual exchange correction

The mass spectra were analyzed as described before (25). Briefly, for HX-MS spectra containing a single peak, the centroid mass was used to determine the average mass for labeled reporter peptides. Spectra with multiple peaks (bimodal at most in this study) were fit with two Gaussian peaks using Microsoft Excel.

Both forward and back exchange occurring during the sample analysis time were taken into account for all the reporter peptides using the method developed by Wetzel et al. (27):

$$\text{corrected deuterium incorporation}: \quad D_{\text{coor}} = m - \text{MW} + \text{BE} - \text{FE}; \tag{1}$$

and

$$\text{forward exchange}: \text{FE} = m_0 - \text{MW}; \tag{2}$$

$$\text{back exchange}: \text{BE} = \text{MW} + N - m_{100}. \tag{3}$$

All the parameters in the equations above have definitions identical the those cited by Kheterpal et al. (27), and the only difference is that they are applied to proteolytic peptides, rather than intact Aβ protein. *MW* is the theoretic mass of each reporter peptide, measured from unlabeled Aβ(1-40) sample with the final dilution step incorporating 0.05% FA in H_2O instead of D_2O/H_2O mixture. m_0 is the measured average mass of unlabeled sample using D_2O-rich solvent dilution described in Materials and Methods. m_{100} is the average mass of peptide from fully labeled Aβ(1-40) sample by dissolving Aβ in D_2O-based PBS for 1 h at room temperature. *m* is the average mass from test samples after certain labeling times. *N* represents the total exchangeable backbone amide protons within each reporter peptide. To account for the 90% Deuterium under our labeling condition, modification to Eq. 1 was made (see below):

$$D_{\text{coor}} = (m - \text{MW} + \text{BE} - \text{FE})/0.9. \quad (4)$$

The fractional deuteration or solvent accessibility (SA) of each reporter peptide was then defined by

$$\text{SA} = \frac{D_{\text{coor}}}{N} \times 100\%. \quad (5)$$

Circular dichroism spectroscopy

All the circular dichroism spectroscopy (CD) measurements were carried out on an Aviv CD spectrometer (Model 215; AVIV Biomedical, Lakewood, NJ) at 25 ± 0.5°C. The path length of the quartz cell is 0.5 mm. The scanning wavelength was 195–260 nm with step size of 1 nm. For each sample, three scans were acquired and averaged. All the presented spectra were corrected by subtracting the baseline spectrum collected for PBS buffer.

Congo Red binding assay

Congo Red (CR) solution (120 μM in PBS buffer) was filtered through 0.22 μm syringe-driven filter three times before use, and then mixed with 100 μM Aβ(1-40) sample in a 96-well plate at a volume ratio of 1:9 (CR vs. Aβ solution). After binding for 45 min at room temperature, absorbance at two wavelengths of 405 nm and 540 nm was measured by SpectraMax Plus^{384} Microplate Reader (Molecular Devices, Sunnyvale, CA). PBS buffer was used as the blank reference. The concentration of Congo Red (mol/L) bound to Aβ sample was determined by Klunk et al. (28).

$$[\text{CR} - A\beta] = A_t^{541}/47,800 - A_t^{403}/68,300 - A_{\text{CR}}^{403}/86,200 \quad (6)$$

A_t^{403} and A_t^{541} are the total absorbance of Aβ(1-40) plus Congo Red at 405 nm and 540 nm, respectively. A_{CR}^{403} is the absorbance of Congo Red alone in PBS at 403 nm. Absorbance values at 405 nm and 540 nm were assumed to be same as those at 403 nm and 541 nm (28).

RESULTS

The assignment of HX labeling behaviors to particular aggregated species

We have reported previously that multiple aggregated Aβ (1-40) species can be distinguished by their degree of solvent accessibility using HX-MS without proteolysis (25). Separate peaks in HX mass spectra were assigned to a particular aggregated species using multiple techniques, including SEC, EM, and AFM as described previously (13,25). Briefly, the bimodal labeling pattern of fresh Aβ(1-40) sample was correlated with the two species of monomer (fully labeled peak) and LMW oligomers (partially labeled peak) that were shown in SEC experiments in similar proportions (13). For Aβ samples aged 4 h and 10 h, one predominant peak with moderate solvent accessibility was observed in HX mass spectra, whereas EM and AFM showed the primary HMW oligomer species to be spherical or disk-like (13,25, and Fig. S3 in the Supporting Material). For 6-day aged, washed fibrils, HX spectra yielded a homogeneous peak with a low degree of deuterium labeling. Although aged Aβ samples are certainly heterogeneous in general, the above conditions yielded predominantly one aggregated species, allowing the assignment of HX behavior for at least the predominant oligomer morphologies listed above.

In the current study, the peptide level solvent accessibility patterns were investigated via enzymatic digestion to show the local structural differences between various aggregated species. To allow comparison with our previous experiments, all the samples were prepared, aged, and labeled with deuterium with the same procedures as our previous study.

Aβ(1-40) proteolysis efficiency and artifactual exchange

Online proteolysis of Aβ(1-40) peptide was carried out with two immobilized acid-compatible enzyme columns operated in tandem, one containing pepsin and the other containing fungal protease type XIII. As shown in Fig. 1, the use of two enzymes with different cleavage preferences provided us with more reporter peptides detectable in the mass spectrum with a high S/N ratio than was reported previously for Aβ (26). The assignments of all the eight reporter peptides were confirmed by running MS/MS mass spectrometry and analyzing the obtained spectra with software TurboSEQUEST. Met^{35} in Aβ(1-40) was not oxidized after our sample preparation as indicated by the absence of an oxidized peak for intact Aβ and reporter peptide 35–40 in our mass spectra (data not shown). As another significant evaluation of our experimental system, both forward and back exchange induced into each reporter peptide during the sample processing time were determined by a series of control experiments as described in Materials and Methods. These control experiments were essential for the precise assessment of the peptide level solvent accessibility for different Aβ(1-40) samples. In our system, the measured back exchange of eight reporter peptides varied between

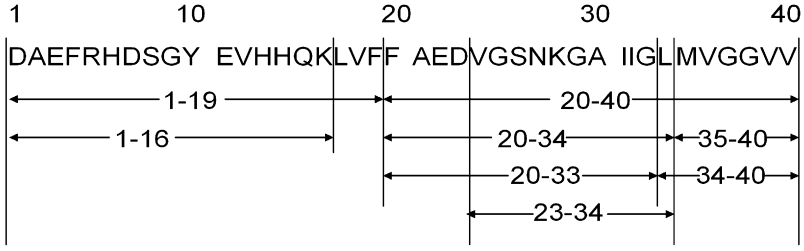

FIGURE 1 Eight reporter peptides from Aβ(1-40) protein observed in HX-MS spectra using sequential immobilized pepsin and fungal protease type XIII enzyme columns. All the peptides were identified according to their mass and charge states and further confirmed by MS/MS.

15.5% and 42.6%, with the two N-terminal peptides 1-16 and 1-19 showing a significantly higher degree of back exchange (38.8% and 42.6%, respectively), and the six C-terminal peptides having a degree of ~30.0% or below. In contrast, the forward exchange was low and relatively constant for all the reporter peptides (0.2%–5.4%).

Solvent accessibility of washed Aβ(1-40) fibrils at proteolytic peptide level

The solvent accessibility of Aβ fibrils has been well investigated at different resolution level by several research groups (25,26,29,30). The re-examination of Aβ(1-40) fibrils here was used to validate our experimental protocol and data analysis by comparing our measurements with two previous independent studies (Supporting Material). In this study, 6-day aged washed Aβ samples were treated as pure fibrils (see preparation in Materials and Methods), which was supported by the observed highly homogeneous labeling distribution in obtained HX-MS spectra both by earlier study of intact Aβ (25) and this peptide level investigation. The representative HX-MS spectra of eight reporter peptides from washed fibrils after 24 h deuterium labeling are shown in the Supporting Material. Deuterium labeling into each proteolytic reporter peptide of fibrils (shown in the fibril column of Table 1) was calculated from centroid mass of HX-MS spectra as described in Materials and Methods. Consistent data of solvent accessibility was found for Aβ(1-40) fibrils either between this and two previous studies or between this and our earlier study (Supporting Material), validating the methodology used.

The general solvent accessibility pattern of washed Aβ (1-40) fibrils is indicated by the deuterium labeling of three nonoverlapping reporter peptides spanning the whole sequence, e.g., reporter peptides 1-19, 20-34, and 35-40 in Table 1. The two terminal regions 1-16 (54.7 ± 2.0% deuteration calculated based on Table 1) and 35-40 (74.0 ± 2.0%) showed a higher degree of solvent accessibility than the central β-structure forming fragment 20-34 (39.3 ± 1.0%) in fibril assembly (31,32). A more detailed pattern of solvent accessibility for Aβ fibrils was also available through the analysis of labeling differences between partially overlapping reporter peptide pairs. For instance, given the deuterium numbers of 8.2 ± 0.3 and 8.8 ± 0.3 measured for reporter peptides 1-16 and 1-19 respectively, the labeling difference of 0.6 ± 0.4 is indicated to arise from residues 17-19, meaning a solvent accessibility of ~20.0 ± 13.3% in this segment. Likewise, the nearly identical deuterium labeling of reporter peptides 20-34 and 23-34 (5.5 ± 0.1 vs. 5.4 ± 0.1) suggests that residues 21–23 are almost fully protected from H/D exchange. However, the labeling status of residue 20 could not be determined based on the above two reporter peptides alone, because the N-terminal residue is no longer an amide and exchanges rapidly with solvent H_2O during analysis. Table 2 (*Fibril column*) shows the deuterium labeling of subpeptides or particular residues for washed fibril sample determined from all the peptide pair comparison.

TABLE 1 Summary of measured deuterium number incorporated into each Aβ reporter peptide from different aggregated states

Fragment	Total exchangeable protons	Corrected deuterium number			
		Monomer*	LMW*	HMW†	Fibril‡
1-16	15	15.2 ± 0.4	15.2 ± 0.4	14.7 ± 0.3	8.2 ± 0.3
1-19	18	18.0 ± 0.4	18.0 ± 0.4	15.6 ± 0.4	8.8 ± 0.3
20-33	13	12.8 ± 0.3	7.7 ± 0.3	5.7 ± 0.2	5.2 ± 0.1
20-34	14	13.9 ± 0.3	8.6 ± 0.3	5.9 ± 0.3	5.5 ± 0.1
23-34	11	10.8 ± 0.3	7.8 ± 0.4	5.7 ± 0.2	5.4 ± 0.3
34-40	6	5.7 ± 0.1§	4.0 ± 0.1¶	3.9 ± 0.1	3.9 ± 0.1
35-40	5	4.8 ± 0.1§	3.7 ± 0.1¶	3.6 ± 0.1	3.7 ± 0.1
20-40	19	19.9 ± 0.2	11.8 ± 0.4	8.9 ± 0.3	8.6 ± 0.3

Uncertainties are based on the SD triplicates.
*Aβ(1-40) monomer and LMW oligomers from fresh sample, labeled for 10 s.
†Spherical HMW oligomers from 4-h aged samples, labeled for 1 h.
‡Washed fibrils from 6-day aged sample, labeled for 24 h.
§Values determined from 1 h labeled fresh sample.
¶Value determined from calculation by Eq. 7.

Solvent accessibility of Aβ(1-40) monomer and LMW oligomers at proteolytic peptide level

The freshly prepared sample of Aβ(1-40) peptide was shown to be a mixture of fully solvent exposed monomer and partially protected LMW oligomers by our earlier HX-MS study (25). The left column of Fig. 2 (reproduced from Qi et al. (25) by permission) shows the HX-MS spectra of undigested fresh Aβ(1-40) sample after three different labeling times. The bimodal HX behavior observed with labeling

TABLE 2 Summary of deuterium number incorporated into Aβ subpeptides or residues from different aggregated states

Residue(s)	Total exchangeable protons	Deuterium incorporation			
		Monomer*	LMW*	HMW†	Fibril‡
1–16§	15	15.2 ± 0.4	15.2 ± 0.4	14.7 ± 0.3	8.2 ± 0.3
17–19¶	3	2.8 ± 0.6	2.8 ± 0.6	0.9 ± 0.5	0.6 ± 0.4
21–23¶	3	3.1 ± 0.4	0.8 ± 0.5	0.2 ± 0.4	0.1 ± 0.3
24–33‖	10	9.7 ± 0.5	6.9 ± 0.6	5.5 ± 0.4	5.1 ± 0.3
34¶	1	1.1 ± 0.4	0.9 ± 0.4	0.2 ± 0.4	0.3 ± 0.1
35¶	1	0.9 ± 0.1	0.3 ± 0.1	0.3 ± 0.1	0.2 ± 0.1
36–40§	5	4.8 ± 0.1	3.7 ± 0.1	3.6 ± 0.1	3.7 ± 0.1

Uncertainties are calculated by error propagation.
*Aβ(1-40) monomer and LMW oligomers from fresh sample, labeled for 10 s.
†Spherical HMW oligomers from 4-h aged samples, labeled for 1 h.
‡Washed fibrils from 6-day aged sample, labeled for 24 h.
§Values are determined from direct measurement of reporter peptides 1-16 and 35-40, respectively.
¶Values are determined from labeling difference between partially overlapping peptide pairs.
‖Value is determined by subtracting the deuterium number of residues 21–23 from reporter peptide 20-33.

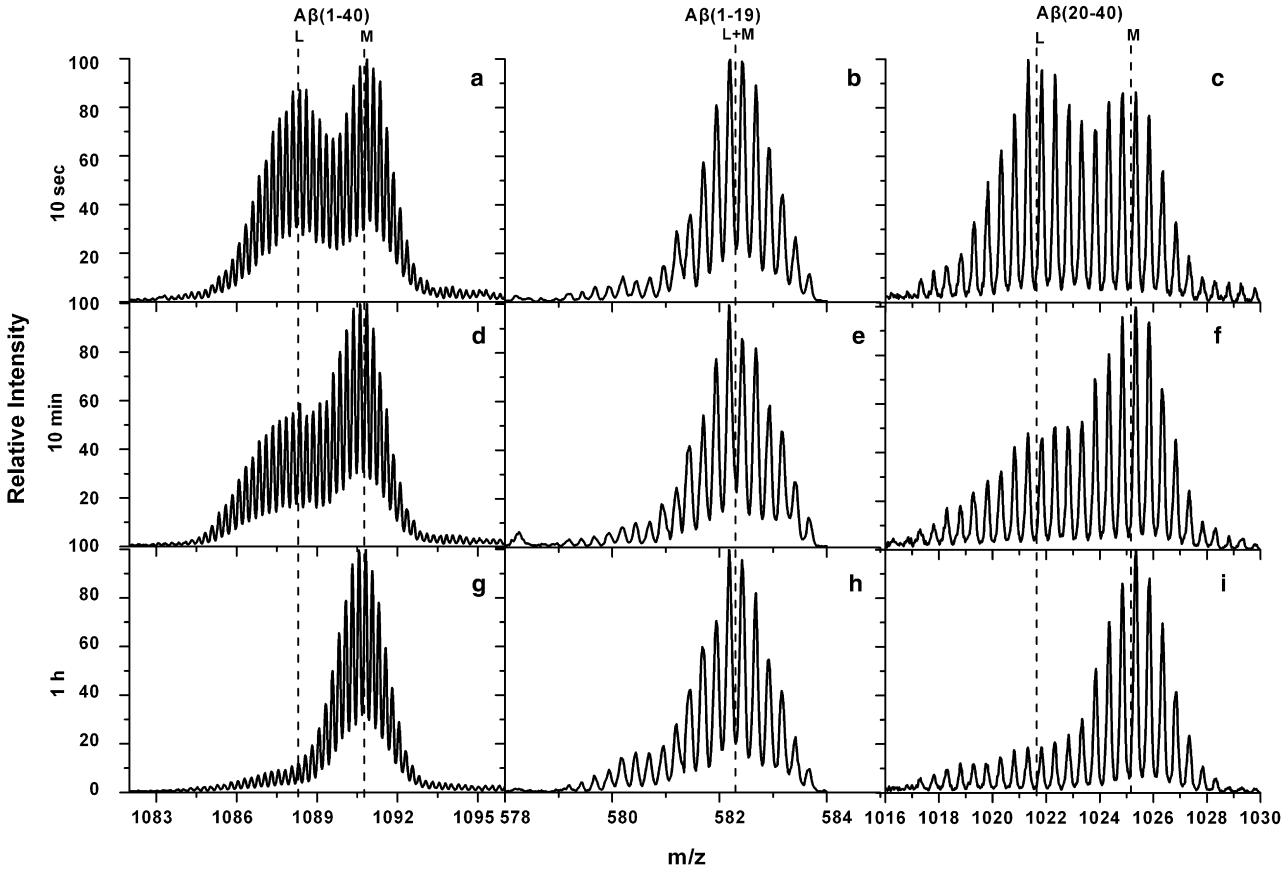

FIGURE 2 Representative HX-MS spectra of intact Aβ(1-40) (*left*), and two reporter peptides 1-19 (*middle*) and 20-40 (*right*) from freshly prepared sample. The labeling time for each sample is marked on the left side of each row of spectra as 10 sec, 10 min and 1 h. The assignments of peaks are marked with L (LMW oligomers) and M (monomer). Intact Aβ(1-40) spectra are reproduced from Qi et al. (25) by permission.

times indicate the presence of two labeling states with distinct solvent accessibility, consistent with the observations by SEC and native PAGE of two species in dynamic equilibrium, monomer and LMW oligomers primarily composed of dimer (13,29). Moreover, the molar ratio of two labeling states shown by a short H/D exchange time (10 s) agreed with the monomer/dimer ratio of ~1:1 by SEC (13). Therefore, the two peaks in Fig. 2, *a* and *b*, are assigned to be fully labeled monomer (high mass peak) and protected LMW oligomers (low mass peak).

To identify the protected region of Aβ peptide in the early formed LMW oligomers, the postlabeled fresh sample was subject to proteolytic cleavage, and the digested peptide mixture was analyzed instead of intact Aβ to determine solvent accessibility patterns. Representative HX-MS spectra of two complementary reporter peptides 1-19 and 20-40 after 10 s, 10 min, and 1 h labeling are shown in the right two columns of Fig. 2. Interestingly, reporter peptide 1-19 displays one single peak in mass spectra at all the labeling times. The calculated deuterium labeling after artifactual exchange correction is 18.0 ± 0.4 (Table 1), equivalent to the maximum value achievable at full deuteration situation of this peptide. This indicates that the N-terminal region spanning residues 1–19 of Aβ(1-40) peptide is flexible and rapidly solvent exposed in both the monomeric and LMW forms found in fresh samples. Similar spectra were observed for reporter peptide 1-16 (data not shown). In contrast, reporter peptide 20-40 shows an abundance transition between two labeling states with increasing labeling times, similar to that observed in intact Aβ(1-40), suggesting that the protected region of Aβ in LMW oligomers is located in C-terminal half region 20-40. The two labeling states were fitted by two Gaussian peaks and gave a corrected deuterium number of 11.8 ± 0.4 and 19.9 ± 0.2 (full deuteration), respectively (Table 1).

To further localize the residues showing HX protection in LMW oligomer structure, the HX-MS spectra of two smaller reporter peptides are shown in Fig. 3. Similarly, reporter peptide 20-34 shows a bimodal HX behavior with varying labeling times. The rate of decrease in the low mass peak with labeling time is comparable with these observed for intact Aβ and reporter peptide 20-40 (Fig. 2). Similar spectra were obtained for reporter peptides 20-33 and 23-34 (data not shown). The deuterium labeling for the two peaks of peptide 20-34 spectra (Fig. 3 *a*) is 8.6 ± 0.3 and 13.9 ± 0.3, respectively (Table 1). On the other hand, the HX-MS

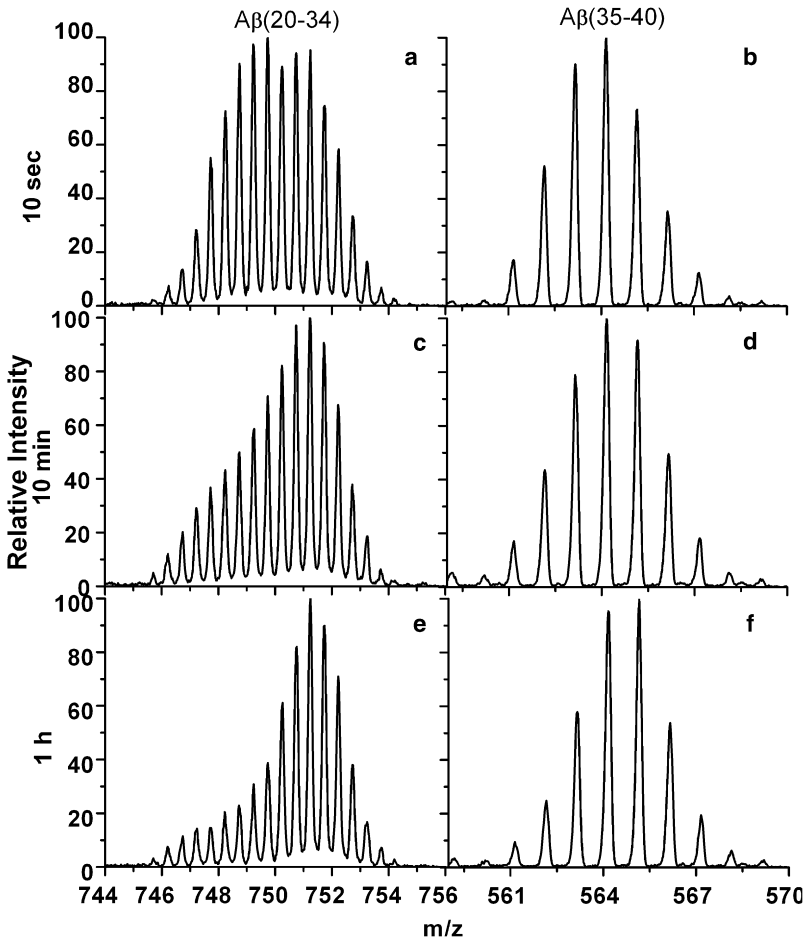

FIGURE 3 Representative HX-MS spectra of reporter peptides 20-34 (*left column*) and 35-40 (*right column*) from freshly dissolved Aβ(1-40) sample. The labeling time for each sample is marked on the left side of each row of spectra as 10 s, 10 min, and 1 h.

spectra of reporter peptide 35-40 seem to be unimodal. However, the calculated centroid mass was found to increase with the labeling time, suggesting the presence of a partially labeled species together with the fully labeled peptide. This is also consistent with a less degree of protection observed for reporter peptide 20-34 (5.3 $\pm$ 0.4 unlabeled residues) relative to reporter peptide 20-40 (8.1 $\pm$ 0.4 unlabeled residues). Therefore, the residues protected from H/D exchange in LMW oligomers are distributed throughout the C-terminal half region spanning sequence 20-40.

Notably, the HX protection observed for either intact Aβ molecule and digested peptides from LMW oligomers had a limited lifetime. In Figs. 2 and 3, the less labeled peaks disappear almost completely after 1 h of labeling both. This suggests that the structure within LMW oligomers causing the solvent protection is not stable for timescales longer than 1 h, either because of rapid association/dissociation equilibrium with fully unfolded monomeric state or large-scale fluctuation in structure sufficient to become solvent exposed in region 20-40.

Because of the low resolution of the protected and unprotected species in reporter peptide 35-40 (Fig. 3 *b*), the deuterium labeling of the less labeled component was calculated in another way as described previously (26). The centroid mass of the entire spectrum is a weighted sum of the partially labeled and fully labeled contributions:

$$M_{\text{ave}} = \alpha_1 M_{\text{PL}} + \alpha_2 M_{\text{FL}}. \quad (7)$$

Where M_{ave}, M_{PL}, and M_{FL} are the centroid mass of the overall isotopic peak distribution, the partially labeled component of LMW oligomers and the fully labeled component of monomer, respectively. a_1 and a_2 are the relative abundances of two differently labeled species in a short labeling time, i.e., Aβ LMW oligomers and monomer fractions in fresh sample.

In Eq. 7, $M_{\text{ave}} = 563.9 \pm 0.1$ was calculated from the 10 s-labeling spectrum of reporter peptide 35-40 (Fig. 3 *b*). $M_{\text{FL}} = 564.5 \pm 0.1$ was determined from the spectrum of reporter peptide 35-40 after 1 h labeling (Fig. 3 *f*), by which time we assumed that LMW oligomer became fully labeled as indicated by the intact Aβ and reporter peptide 20-34 spectra (Fig. 2). The relative abundance $a_1 = 0.65 \pm 0.03$ and $a_2 = 0.35 \pm 0.03$ were determined from the deconvolution of the better resolved spectrum of reporter peptide 20-34 (Fig. 3 *a*). With these values, a centroid mass of 563.6 $\pm$ 0.1 for the partially labeled component was determined, corresponding to a deuterium labeling of 3.7 $\pm$ 0.1 after

correction for reporter peptide 35-40. The same analysis was carried out to gain the deuterium labeling value for reporter peptide 34-40 shown in Table 1.

Solvent accessibility of HMW oligomers at proteolytic peptide level

Like LMW oligomers observed in fresh Aβ samples, HMW oligomers exist in mixtures together with other Aβ species and cannot be completely isolated. Consequently, we focused on aging conditions that provided a predominant fraction of these oligomers and used HX-MS to distinguish these oligomers from the other species. Our earlier studies of intact Aβ (1-40) by AFM and EM showed that HMW oligomers became the predominant species in 4–10 h aged samples and coexisted with mature fibrils in 72 h aged samples (13,25). These microscopy results allowed peaks in HX-MS spectra of intact Aβ (Fig. 4, *left column*; reproduced from Qi et al. (25) by permission) to be assigned. Three distinct peaks were observed to transform in their abundance with respect to the aging time, while keeping the individual *m/z* unchanged. The peak with the lowest m/z (~1084.8) was the highly protected Aβ fibrillar species mainly found in the 6-day washed sample (Fig. 4 *i*) and 72-h aged sample (Fig. 4 *e*). The minor, high mass peak appearing in 4-h and 72-h samples had a centroid position of ~1090.4, consistent with a monomeric state with full deuteration. Finally, the peak with an intermediate *m/z* (~1087.1) was assigned to HMW oligomers according to their relative abundance in the 4-h and 72-h aged samples observed in AFM images (25).

The discrimination of different aged samples by intact Aβ HX-MS discussed above facilitated the analysis of solvent accessibility at the proteolytic peptide level. However, it should be noted that as described in Materials and Methods, all the aged samples were subjected to centrifugation to concentrate the large Aβ aggregates for peptide level analysis and meanwhile reduce the contribution of LMW oligomers

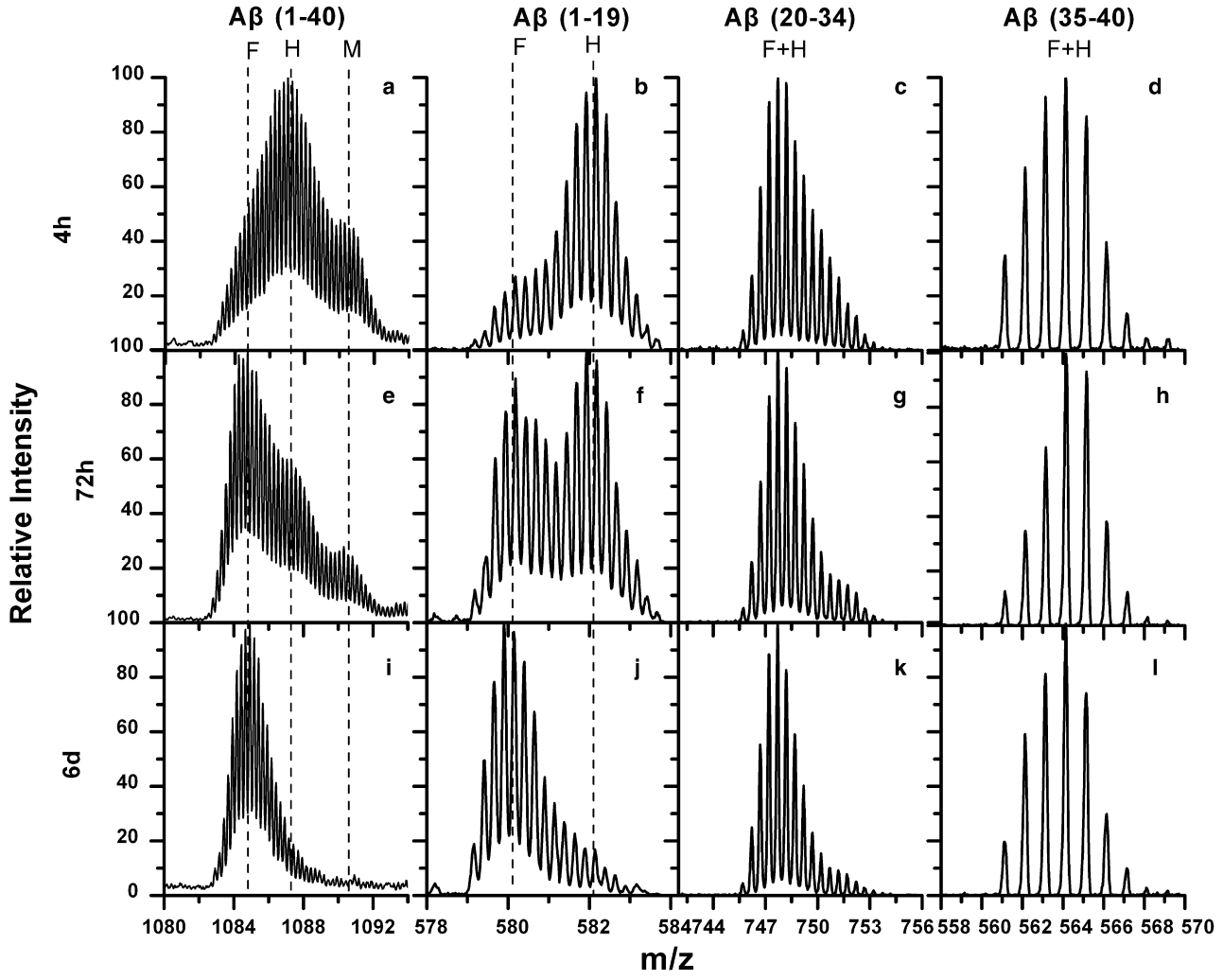

FIGURE 4 Representative HX-MS spectra of different aged Aβ samples after 1 h deuterium labeling. Each row represents one sample aging time denoted at left. Each column presents one report peptide denoted on the top. The assignments of peaks to different species are marked as F (fibrils), H (HMW oligomers), and M (monomer).The intact Aβ spectra in the left column are reproduced from Qi et al. (25) by permission.

and monomer. For analysis convenience, the HX-MS spectra of three selected reporter peptides (1-19, 20-34, and 35-40) are also shown in Fig. 4. The simplest HX behavior was observed for 6-day washed fibrils, which showed relatively homogeneous labeling distributions for the three reporter peptides (Fig. 4, *j–l*). Similarly, the reporter peptides from 4-h aged samples have predominantly one peak (Fig. 4, *b–d*), consistent with the predominance of one peak due to HMW oligomers in the intact spectrum (Fig. 4 *a*). Reporter peptides 20-34 and 35-40 showed centroid peak positions similar to those obtained for washed fibrils. The main cause for the difference in labeling of intact HMW oligomers would seem to be within reporter peptide 1-19, which was labeled to a much higher degree in 4-h samples (Fig. 4 *b*) than 6-day washed fibrils (Fig. 4 *j*). The 72-h aged samples showed very similar HX-MS spectra to the other two aged samples in reporter peptides 20-34 and 35-40. However, two well resolved peaks were observed for reporter peptide 1-19, with the low mass peak having a close centroid position to the single peak from 6-day washed fibrils, and the high mass peak to the major peak from 4-h aged sample. The other reporter peptides showed similar behavior as depicted in Fig. 4, with peptide 1-16 being similar to 1-19; peptides 20-40, 20-33, and 23-34 being similar to 20-34; and peptide 34-40 being similar to peptide 35-40. The number of deuteron labeled in the reporter peptides of HMW oligomers were calculated using the 4-h spectra (Table 1). As a consistency check, the total deuterium number of three reporter peptides 1-19, 20-34, and 35-40 for HMW oligomers are (25.1 $\pm$ 0.5), slightly higher than the direct measurement from our early intact Aβ analysis (23.3 $\pm$ 0.9) (25).

The HX-MS spectra of 4-h aged sample (Fig. 4, *top row*) provide some additional insight regarding the structure of Aβ(1-40) HMW oligomers. Reporter peptide 20-34 shows an asymmetric isotopic peak envelope with a high mass tail having a deuterium labeling intermediate between LMW and HMW oligomers. Similar mass spectra were also observed for two other reporter peptides 20-35 and 20-40 (data not shown). The tails in HX-MS spectra associated with C-terminal reporter peptides may indicate a heterogeneous distribution of solvent accessibility in this region for HMW oligomers formed in 4-h aged sample. Taking into account the significant variance in the size dimension of HMW oligomers observed by AFM (25), a correlation between the assembly size of HMW oligomers and the degree of solvent protection might be present. For example, addition of more Aβ peptides into the oligomer structure could lead to a more rigid or ordered assembly pattern, thus a higher extent of solvent protection in the HMW oligomers.

Comparison of peptide level solvent accessibility pattern for different Aβ(1-40) aggregated states

The solvent accessibility pattern of Aβ peptide in different aggregated states can be compared between each other. Fig. 5 (data based on Table 2) summarizes the peptide level HX results of four Aβ aggregated forms: monomer, LMW oligomers, HMW oligomers, and fibrils. The results are presented in two formats: 1), the solvent accessibility pattern for each aggregated state is shown in Fig. 5 *a*), particular fragments with significant difference in solvent accessibility between two sequential aggregated states are identified in Fig. 5 *b*. Due to the rapid exchange rates for the fresh Aβ samples and additional isolation steps used for the aged samples, the solvent accessibility for different samples were not compared at a common, short labeling time. This prevents a precise quantitative comparison of residue numbers showing HX protection under identical labeling and sample workup conditions. However, the fact that all the reporter peptides show a decreased degree of solvent accessibility with the increasing aggregated states even though they are subject to a longer labeling time means the actual differences in degree of labeling are even more significant.

From Fig. 5 *a*, we can see that LMW oligomers experience a reduction in solvent accessibility in the C-terminal region 21-40 as compared to the monomer sample. As LMW oligomers are converted to HMW oligomers, solvent accessibility is further reduced in residues 21-34; the region of protection is also extended to residues 17-19. However, both LMW and HMW oligomers retain nearly full solvent accessibility in the N-terminal region 1-16. This N-terminal reporter peptide remains quite solvent exposed until the development of fibrils, in which about half of its residues become protected from H/D exchange. By comparing the solvent accessibility patterns for the four states, Fig. 5 *b* highlights how solvent protection spreads from the C-terminus to the N-terminus with increasingly aggregated states.

Secondary structure changes during Aβ aggregation

The secondary structure changes occurring during Aβ aggregation were examined by CD spectroscopy as shown in Fig. 6. At diluted low peptide concentration (10 μM), where the monomeric species was favored thermodynamically, Aβ adopted primarily random coil conformation (Fig. 6, *curve 1*). In contrast, a shallow band around 210–220 nm was observed for the elevated 100 μM fresh sample (Fig. 6, *curve 2*), where we have already shown a substantial fraction of oligomeric species were formed (13,25). After incubation of various times, all the aged samples (100 μM) display far stronger characteristic absorbance of β-sheet structure around 215–220 nm, with a continuous increase in the signal at 218 nm $[\theta]_{218}$ over aging time. Light scattering caused by large Aβ aggregates in aged samples could be considered to be a potential influence on these results. However, these effects should not be significant in our study because the CD signal was not distorted obviously by existing scattering noise. The fibril-containing samples (Fig. 6, *curves 5* and *6*) remained a major β-structure characteristic absorbance as smaller oligomeric samples with intermediate aggregation. Moreover, the dynode voltage was far below 500 V for all samples,

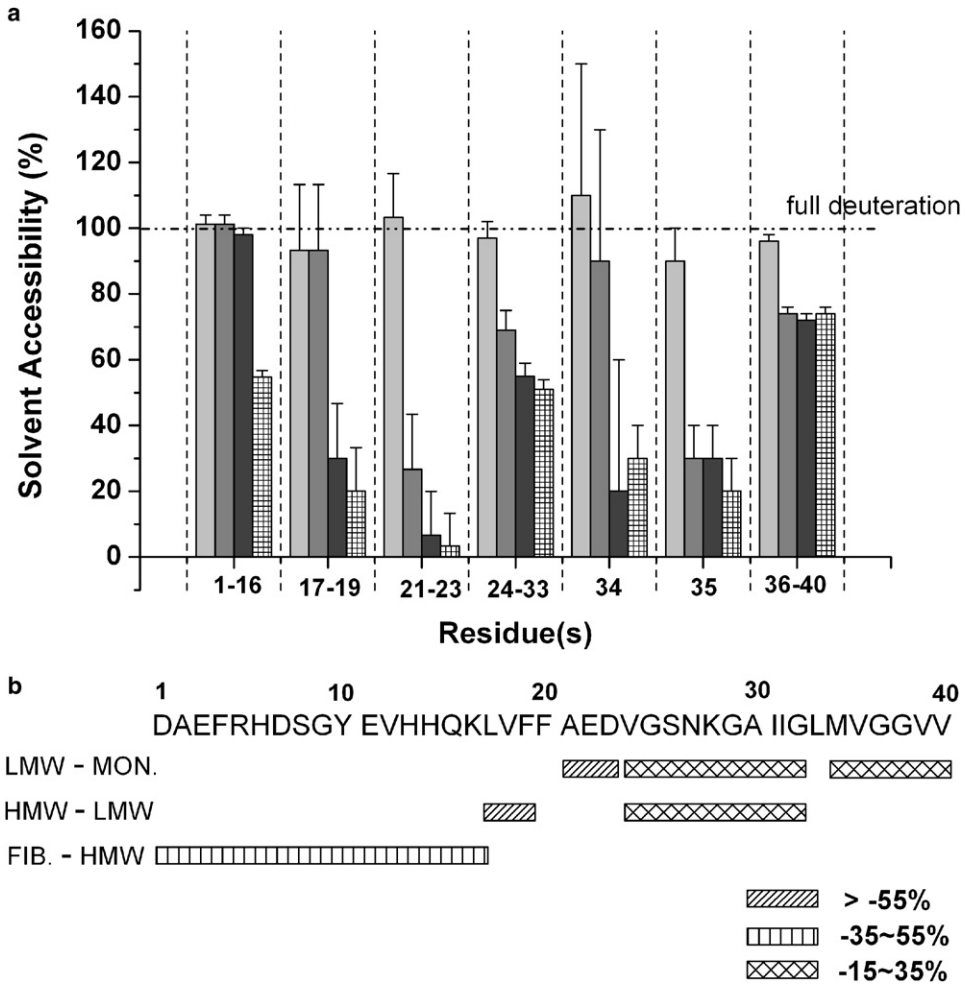

FIGURE 5 Presentation of peptide level solvent accessibility for Aβ(1-40). (*a*) The peptide level solvent accessibility pattern of Aβ(1-40) in different aggregated states. The deuterium labeling times for monomer (*light gray*) and LMW oligomers (*gray*) from fresh sample, HMW oligomers (*dark gray*) from 4-h aged sample, and fibrils (*squared*) from 6-day washed sample are 10 s, 1 h, and 24 h, respectively. The horizontal dash dot line corresponds to 100% solvent accessibility at full deuteration. (*b*) Aβ reporter regions with significant difference in solvent accessibility between two sequential aggregated states. Bars span peptide regions that are significantly different (significance level α is 0.05) for three pairwise comparisons: (LMW-MON) LMW oligomers versus monomer, (HMW-LMW) HMW versus LMW oligomers, and (FIB-HMW) fibrils versus HMW oligomers. No bars are shown for regions without significant differences.

indicating a consistently low degree of contribution from scattering noise. Thus, although light scattering effects might still affect a quantitative deconvolution to determine small changes in secondary structure content, they should not affect the qualitative conclusion that β structure is increasing with aging time. Given the relatively constant abundance of monomeric Aβ in all the aged samples (25), the growth of the β-sheet content may reflect the extension of β-strands in Aβ peptide when the mature fibril structure develops from HMW oligomers.

Congo Red is a histological dye usually used to monitor the growth of amyloid fibrils. However, some forms of Aβ intermediates were also found to show a binding capacity (34). In this study, the amount of Congo Red bound to different Aβ samples was measured as an indicator of the ordered cross-β structure present in the formed predominant aggregated states. As expected, Fig. 7 shows the fresh sample has a low Congo Red binding capacity, indicating the lack of ordered cross-β structure in both Aβ monomer and LMW oligomers. For the samples of short aging times (1 and 2 h), a gradual increase in CR binding was observed. Samples aged for 4 h and 10 h, in which HMW oligomers become the dominant species, reached a plateau of Congo Red binding. Thereafter, no significant change was observed for even longer aged samples, though the amount of fibrillar species grew substantially in 72-h and 6-day aged samples. This result suggests that Congo Red is not able to distinguish the intermediate HMW oligomers and maturely developed amyloid fibrils.

DISCUSSION

The understanding of Aβ aggregation at molecular level is central to the development of therapeutic strategies to address Alzheimer's disease. To date, considerable efforts have been exerted to investigate the aggregation process (4,8,34). However, most previous studies were concentrated on either the late fibril growth phase or the large, and dynamically stable Aβ aggregates such as protofibrils and fibrils (17,26,34), whereas the structure of the earlier oligomers are much less explored. For example, HX-MS has been applied to study Aβ aggregates, but only to fibrils (29,35) and chemically stabilized protofibrils (26,36). HX detected by NMR has been applied only to fibrils as well (30). We report the local solvent accessibility of two intermediate oligomers (LMW and HMW oligomers) along with the monomeric and fibrillar Aβ, using HX-MS with proteolytic

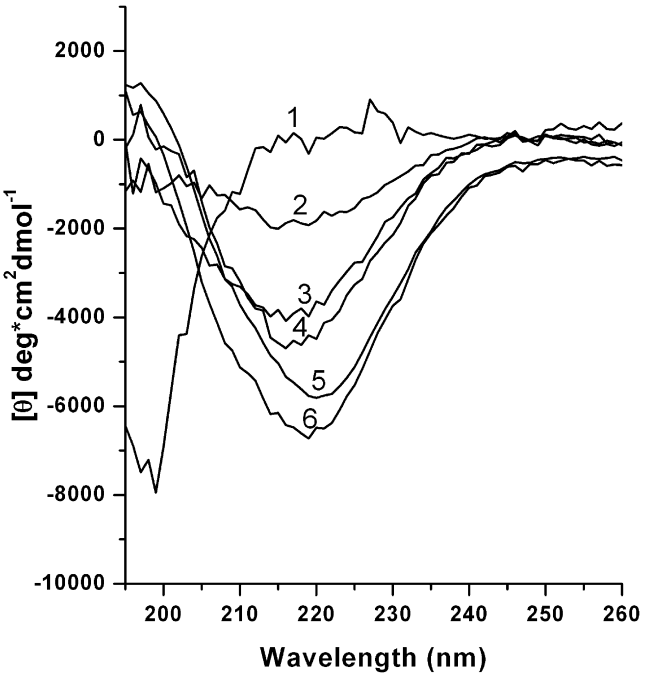

FIGURE 6 The Aβ(1-40) secondary structure changes during aggregation shwon by CD. The investigated samples are: fresh sample 10 μM (*curve 1*), fresh sample 100 μM (*curve 2*), 4-h aged sample (*curve 3*), 10-h aged sample (*curve 4*), 72-h aged sample (*curve 5*), and 6-day aged sample (*curve 6*). All the aged samples were measured at concentration 100 μM.

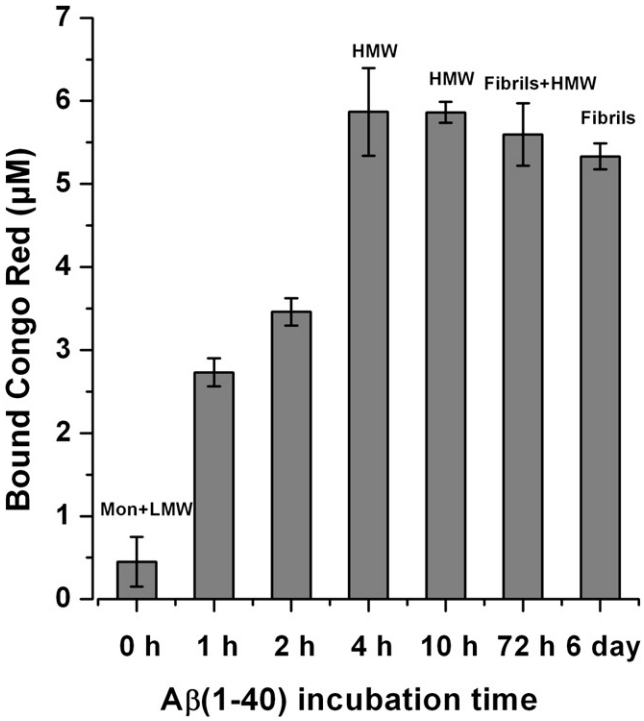

FIGURE 7 Congo Red binding changes with Aβ(1-40) sample aging time. The error bar was calculated from measurements on triplicates. Designations above each bar indicate the type of Aβ(1-40) aggregates present in sample, as indicated by complementary AFM and EM studies under the same conditions and the intact HX-MS labeling (13,25).

digestion to increase spatial resolution. Although the analysis of HX kinetics is not as quantitative as has been applied to HX-NMR studies of nonaggregating proteins, mass spectrometry detection facilitates the resolution and analysis of oligomeric species present in mixtures. This is an important issue for distinguishing the structural features of transient Aβ oligomers.

The Aβ(1-40) subpopulation distribution with respect to aging time shown by HX-MS and AFM in our previous study (25) indicated a progressive aggregation pathway started with unfolded monomer and ended with mature fibrils with two intermediate oligomeric species. In this aggregation process, the initial self-association occurs readily on sample dissolution, leading to the formation of LMW oligomers in rather rapid equilibrium with monomer (8,13). During the subsequent oligomer growth phase, Aβ oligomers grow in assembly sizes and coincide with a gradual increase in structure stability indicated by HX-MS (25). Though a further detailed discussion of the aggregation mechanism and kinetics is beyond our scope, the peptide level HX-MS analysis can show the local changes in solvent accessibility that accompanies formation of each species.

Introduction of solvent protected β-sheet structure into the C-terminal region 20-40 during the early oligomerization process

The Aβ peptide is generally considered to be fully unfolded in the monomeric state in aqueous solution (37,38). Our HX data experimentally confirmed that a significant portion of monomeric Aβ(1-40) in fresh sample was fully solvent accessible within the shortest (10 s) labeling time (Fig. 2). Under our aggregation conditions, however, we also observed a comparable fraction of oligomeric Aβ in freshly prepared sample exhibiting solvent protection in reporter peptides 20-34 and 35-40 (Fig. 3). According to the CD spectra of fresh Aβ samples under two concentration conditions (Fig. 6), β-sheet structure is introduced into the early formed LMW oligomers to some extent when the randomly coiled Aβ monomers are associated together. Thus, one source for the H/D exchange protection in LMW oligomers could be attributed to the β-sheet structure contact between Aβ peptides. Because the N-terminal region 1-19 remains the full solvent accessibility in oligomeric structure, the β-sheet structure contact in LMW oligomers is most likely located in the hydrophobic C-terminal region of Aβ peptide. In particular, residues 21–23, 35, and part of fragments 24–33 and 36–40, all showing significant solvent protection (Fig. 5 *a*), are probably the early residues involved in the initiation of β-strands in Aβ peptide. These residues distribute throughout sequence 20-40, raising the possibility that the two β-strands present in the structural model of mature Aβ(1-40) fibrils (strands at residues 12-24 and 30-40, respectively according to Tycko et al. (31)) are formed in a partially concerted and not purely sequential manner.

Interestingly, Fig. 5 indicates that residues 21–23 and 35 are among the first residues undergoing large reductions in solvent accessibility in the early formed LMW oligomers. This is a bit surprising given that adjacent residues (e.g., 17–20, 24, 31–34, and 36–40) are more hydrophobic. These residues include the central hydrophobic core 17-21 of particular significance in Aβ fibril formation (32,39–41). Why might this be the case? First, it should be noted that Fig. 5 shows solvent accessibility averaged over reporter peptides. Peptide 24-33 shows a smaller average reduction in solvent accessibility (~30%), but this could involve a short stretch of concentrated, reduced solvent exposure near 21-23 or 35.

There are other reasons to believe that residues 21–30 might be more important than residues 17–20 early in the oligomerization process. Limited proteolysis experiments show residues 21–30 are less solvent exposed than residues 17–20 (42) consistent with our observations. Meanwhile, there are studies pointing to a new notion that the formation of β-turn structure in region 21-30 nucleates the folding process of Aβ monomer, and initiates the molecular association to LMW oligomers (43,44). In this view, the electrostatic interaction between Lys^{28} and Glu^{22}/Asp^{23} are crucial in stabilizing the early compact molecule structure. If such an interaction is occurring in an intermolecular manner as in the final fibril structure, i.e., the residues Lys^{28} and Glu^{22}/Asp^{23} forming salt bridges are from two different Aβ molecules (16,31), these charged residues would also play a significant role in facilitating the fast oligomerization process in the early stage. Therefore, the solvent protection for residue 21–23 in our observation could be a result of this initial folding and association process mainly occurring in region 21-30. The hydrophobic core residues 17–20 may show more importance in the late aggregation stage by forming in-register cross-β structure, leading to complete loss of solvent accessibility in these residues in large aggregated forms such as HMW oligomers and fibrils described below.

Development of fibril-like ordered β-sheet structure within residues 17–34 during oligomer growth phase

HMW oligomers dominant in the 4–10 h aged samples showed a significant shift to the elevated β-sheet content (Fig. 6) and Congo Red binding (Fig. 7) relative to LMW oligomers in the freshly dissolved sample. These two measurements indicate a more ordered and extended β-sheet assembly in the growing oligomeric structure. In the parallel HX analysis, a significant reduction in solvent accessibility was only observed within region 17-34 (Fig. 5 *b*), the major portion of β-strand forming region in Aβ(1-40) peptide (31,32). These results suggest that the local β-structural development in region 17-34 may characterize the structure change during oligomer growth stage. In fact, Aβ molecules constructing HMW oligomers showed an indistinguishable solvent accessibility pattern from these in fibrillar structure in the C-terminal region 17-40 (Fig. 5 *b*), strongly indicating the development of fibril-like assembly features in 4–10 aged HMW oligomers. The structural similarity between large spherical oligomers and mature fibrils in the C terminus has also been suggested by one early solid state NMR study of captured intermediate Aβ(1-40) oligomers (45). From LMW oligomers to HMW oligomers, the trend toward more ordered assembly of Aβ peptides within oligomer structure as it grows has been suggested by multiple molecular simulation studies of variant Aβ subpeptides (46–48), though direct experimental evidence is still lacking. The change in the peptide assembly pattern in oligomer structures can lead to the observed distinct structural stabilities for LMW oligomers and HMW oligomers. HMW oligomers seem to have a lower rate in molecular dissociation or large-scale structure fluctuation compared to LMW oligomers as evidenced by the preserved solvent protection after 1 h exchange (Figs. 2 and 4).

Extension of solvent exclusive β-sheet structure into the N-terminal region 1-16 on fibril formation

The structure of Aβ(1-40) fibrils have been studied extensively by assessment of HX solvent accessibility at different resolution levels from multiple research groups (25,26,30). Consistent results were obtained in this study (Supporting Material), indicating that the slightly different sample preparation protocols result in largely equivalent fibrils. In addition, relatively good agreement was also found between our solvent accessibility profile of washed fibrils (Fig. 5 *A*) and the 3D structural model proposed by Tycko et al. (31) based on solid state NMR data. The residue numbers with deuterium labeling within peptide 1-16 and 23-34 agree with the lengths of disordered N-terminus and β-turn linker in Tycko's fibril model, respectively. The two segments 17-23 and 34-35 showing most HX protection are both located entirely within the two intramolecular β-strands of fibrils. However, the disagreement between two studies is also observed in the C-terminal region spanning residues 35–40, which has been noted and discussed previously by Wetzel et al. (26). The unexpectedly elevated solvent accessibility in the C-terminal segment 35-40, despite its high hydrophobicity, could be attributed to the lack of a rigid assembly structure in this region even in maturely developed fibrils, which has also been suggested by limited proteolysis (49), proline and cysteine scanning mutagenesis (32,50), and HX-NMR (30).

Relative to the aggregated form of HMW oligomers, fibrillar Aβ only differs by a significantly reduced solvent accessibility in the N-terminal region 1-16 (Fig. 5 *b*). The small change in local solvent accessibility is surprising given the major change in aggregate morphology of our HMW oligomers to mature fibrils. Our previous analysis by EM and AFM indicates our HMW oligomers are predominantly spherical or disk-like in morphology, with 9–25 nm lateral

dimension, greater than the observed diameter of typical fibrils (13,25). These morphologies are also predominant in the current samples (see new EM images in Fig. S3). Other groups have also observed such morphologies at intermediate stages of aggregation (18–20). Shorter fibrils/protofibrils may be present and may be important intermediates in the process of fibril formation; they are just not the predominant species at 4–10 h under our aggregation conditions. Thus, at least under some aggregation conditions, there is significant restructuring in the aggregates from spheres or disks to fibrils.

Why might there be such a small difference in solvent accessibility patterns when the morphologies of spherical oligomers are so different from fibrils? One explanation would be that HMW oligomers and fibrils are constructed by building blocks that are very similar in molecular level β-sheet structures, but different arrangements of such structures that have weak solvent protection between them. Two previous studies, one conducted by using high resolution AFM (18), and the other by molecular simulation (52), support this interpretation. They proposed disk-like or annular structural models for intermediate oligomers, in which Aβ molecules have the same fundamental β-hairpin structure as those in fibrils. Our measurements of identical, reduced solvent accessibility in region 17-40 suggests that the fundamental structure of building molecules in HMW oligomers and fibrils is located in the C-terminal beta-strand forming region, in good agreement with these two oligomer models. The solvent accessibility reduction within region 1-16 in fibrils could be due to extension of β-sheet structure into the mainly disordered N-terminus. Such an extension of β strands would be consistent with our measured increases in β-sheet content (Fig. 6) and the fibril model obtained by Tycko et al. (31) using solid state NMR.

The structure features of HMW oligomers and correlation with their high neurotoxicity

The structural data of our HMW oligomers can be related to previous models of large spherical Aβ oligomers. First, our HX data disagree with the micelle-like structure model proposed for HMW oligomers (10,53). According to that model, the C terminus of Aβ peptides in large oligomer structure is assumed to be deeply buried in the interior hydrophobic core, thus solvent shielded to a greater extent than in the fibrillar state (53). However, our observations show that the C-terminal reporter peptide 35-40 from HMW oligomers is highly solvent exposed in all the three aggregated states, second only to the N-terminal peptide 1-16 in HMW oligomer structure (Table 1).

Second, the HMW oligomers formed under our Aβ(1-40) aggregation conditions seem to be structurally different from the calmidazolium chloride (CLC) stabilized protofibrils investigated by Wetzel et al. (26,36). Though these two aggregated forms have a similar overall solvent accessibility based on intact Aβ HX measurement, the peptide level solvent accessibility pattern differs significantly between each other. In our measurement, 23.3 $\pm$ 0.9 deuterium can be labeled into HMW oligomers within 1 h compared to 26.2 $\pm$ 1.0 deuterium into CLC-stabilized protofibrils after 1 day exchange. The deuterium labeling into Wetzel's protofibrils changed only slightly with the labeling time, and decreased to between 24 and 25, an extent of labeling closer to our data, if the labeling time was shortened to 1 h (36). Our HMW oligomers showed a significantly higher degree of deuterium labeling (15.6 $\pm$ 0.4) than Wetzel's protofibrils (12.4 $\pm$ 0.6) in reporter peptide 1-19, but a lower degree in reporter peptide 20-34 (5.9 $\pm$ 0.3 for HMW oligomers vs. 9.5 $\pm$ 0.4 for protofibrils) (26). Nevertheless, both our HMW oligomers and Wetzel's CLC-stabilized protofibrils show some basic fibril-like structural features, such as Congo Red binding ability (Fig. 7) and being rich β-sheet structure (Fig. 6). This indicates that HMW oligomers might be a certain form of transient precursor leading to protofibrils and fibrils, for instance, the building blocks to form protofibril structure (7).

Our HX data together with CD measurements also provide what we believe is new insight into the structure basis responsible for the varying degrees of neurotoxicity associated with distinct aggregated Aβ forms (10,13,24). First, it has been suggested that the neurotoxicity of Aβ aggregation is correlated with the development of β-sheet structure in the formed aggregate structure (54). Consistent with that, Aβ monomer and LMW oligomers in freshly prepared sample that showed almost no effect on SY5Y cell viability (13) have little or no β-sheet secondary structure. As for the other two aggregated forms (HMW oligomers and fibrils), both developed substantial β-sheet structure. However, the additional structural difference in the N-terminal region between HMW oligomer and fibril may lead to the observed different neurotoxicity (13). As shown in Fig. 5 *b*, the maturely developed Aβ fibrils differ mainly from HMW oligomers by a more solvent shielded N-terminal region 1-16, where most charged residues are located. As a consequence, the electrostatic interaction between Aβ fibrils and cell membrane might be attenuated. Reducing electrostatic interactions generally between Aβ and membrane has been demonstrated to cause a reduction in the Aβ peptide toxicity (55). Another proposed mechanism of Aβ neurotoxicity involves generation of reactive oxidative species (ROS), caused by binding of metal ions such as Fe^{2+} and Cu^{2+} to Aβ peptides at sites His^{6}, His^{13}, and His^{14} (56). The solvent shielded structure of peptide 1-16 in Aβ fibrils may block the access of metal ions to these binding sites, particularly His^{13} and His^{14}, and thus inhibit the pathway of ROS generation in vivo. Conversely, the highly neurotoxic HMW oligomers have a more flexible and solvent accessible N-terminus, which allows the electrostatic interaction of Aβ peptides with membrane and metal ion binding.

In summary, the peptide level HX-MS has been successfully applied to the Aβ(1-40) aggregation system. The structural differences between multiple aggregated states were identified at a high spatial resolution. A correlation between local structure features and neurotoxicity of Aβ peptide at different aggregated forms was implied, providing what we believe is new insight for the rational development of therapeutic strategies for AD.

SUPPORTING MATERIAL

HX-MS method validation and three figures are available at http://www.biophysj.org/biophysj/supplemental/S0006-3495(08)00088-X.

We gratefully thank Ben Keshet for providing the new EM images.

This study is supported by grant R01 NS042686 from the National Institutes of Health (T.A.G., E.J.F.).

REFERENCES

1. Hardy, J. A., and G. A. Higgins. 1992. Alzheimer's disease—the amyloid cascade hypothesis. *Science*. 256:184–185.
2. Hardy, J., and D. J. Selkoe. 2002. Medicine—the amyloid hypothesis of Alzheimer's disease: progress and problems on the road to therapeutics. *Science*. 297:353–356.
3. Ban, T., and Y. Goto. 2006. Direct observation of amyloid growth monitored by total internal reflection fluorescence microscopy. *Methods Enzymol*. 413:91–102.
4. Blackley, H. K. L., G. H. W. Sanders, M. C. Davies, C. J. Roberts, S. J. B. Tendler, et al. 2000. In-situ atomic force microscopy study of beta-amyloid fibrillization. *J. Mol. Biol.* 298:833–840.
5. Chen, X. G., S. K. Brining, V. Q. Nguyen, and A. L. Yergey. 1997. Simultaneous assessment of conformation and aggregation of beta-amyloid peptide using electrospray ionization mass spectrometry. *FASEB J*. 11:817–823.
6. Goldsbury, C., P. Frey, V. Olivieri, U. Aebi, and S. A. Muller. 2005. Multiple assembly pathways underlie amyloid-beta fibril polymorphisms. *J. Mol. Biol.* 352:282–298.
7. Harper, J. D., S. S. Wong, C. M. Lieber, and P. T. Lansbury. 1999. Assembly of A beta amyloid protofibrils: an in vitro model for a possible early event in Alzheimer's disease. *Biochemistry*. 38:8972–8980.
8. Pallitto, M. M., and R. M. Murphy. 2001. A mathematical model of the kinetics of beta-amyloid fibril growth from the denatured state. *Biophys. J*. 81:1805–1822.
9. Lomakin, A., D. B. Teplow, D. A. Kirschner, and G. B. Benedek. 1997. Kinetic theory of fibrillogenesis of amyloid beta-protein. *Proc. Natl. Acad. Sci. USA*. 94:7942–7947.
10. Kayed, R., E. Head, J. L. Thompson, T. M. McIntire, S. C. Milton, et al. 2003. Common structure of soluble amyloid oligomers implies common mechanism of pathogenesis. *Science*. 300:486–489.
11. Bucciantini, M., E. Giannoni, F. Chiti, F. Baroni, L. Formigli, et al. 2002. Inherent toxicity of aggregates implies a common mechanism for protein misfolding diseases. *Nature*. 416:507–511.
12. Lambert, M. P., A. K. Barlow, B. A. Chromy, C. Edwards, R. Freed, et al. 1998. Diffusible, nonfibrillar ligands derived from A beta(1-42) are potent central nervous system neurotoxins. *Proc. Natl. Acad. Sci. USA*. 95:6448–6453.
13. Lee, S., E. J. Fernandez, and T. A. Good. 2007. Role of aggregation conditions in structure, stability, and toxicity of intermediates in the A beta fibril formation pathway. *Protein Sci.* 16:723–732.
14. Kirkitadze, M. D., M. M. Condron, and D. B. Teplow. 2001. Identification and characterization of key kinetic intermediates in amyloid beta-protein fibrillogenesis. *J. Mol. Biol.* 312:1103–1119.
15. Antzutkin, O. N., R. D. Leapman, J. J. Balbach, and R. Tycko. 2002. Supramolecular structural constraints on Alzheimer's beta-amyloid fibrils from electron microscopy and solid-state nuclear magnetic resonance. *Biochemistry*. 41:15436–15450.
16. Luhrs, T., C. Ritter, M. Adrian, D. Riek-Loher, B. Bohrmann, et al. 2005. 3D structure of Alzheimer's amyloid-beta(1-42) fibrils. *Proc. Natl. Acad. Sci. USA*. 102:17342–17347.
17. Petkova, A. T., W. M. Yau, and R. Tycko. 2006. Experimental constraints on quaternary structure in Alzheimer's beta-amyloid fibrils. *Biochemistry*. 45:498–512.
18. Mastrangelo, I. A., M. Ahmed, T. Sato, W. Liu, C. Wang, et al. 2006. High-resolution atomic force microscopy of soluble Abeta42 oligomers. *J. Mol. Biol.* 358:106–119.
19. Bitan, G., M. D. Kirkitadze, A. Lomakin, S. S. Vollers, G. B. Benedek, et al. 2003. Amyloid beta-protein (Abeta) assembly: Abeta 40 and Abeta 42 oligomerize through distinct pathways. *Proc. Natl. Acad. Sci. USA*. 100:330–335.
20. Goldsbury, C. S., S. Wirtz, S. A. Muller, S. Sunderji, P. Wicki, et al. 2000. Studies on the in vitro assembly of A beta 1-40: implications for the search for A beta fibril formation inhibitors. *J. Struct. Biol.* 130:217–231.
21. Harper, J. D., S. S. Wong, C. M. Lieber, and P. T. Lansbury. 1997. Observation of metastable A beta amyloid protofibrils by atomic force microscopy. *Chem. Biol*. 4:119–125.
22. Harper, J. D., C. M. Lieber, and P. T. Lansbury, Jr. 1997. Atomic force microscopic imaging of seeded fibril formation and fibril branching by the Alzheimer's disease amyloid-beta protein. *Chem. Biol*. 4:951–959.
23. Walsh, D. M., A. Lomakin, G. B. Benedek, M. M. Condron, and D. B. Teplow. 1997. Amyloid beta-protein fibrillogenesis—detection of a protofibrillar intermediate. *J. Biol. Chem.* 272:22364–22372.
24. Kayed, R., Y. Sokolov, B. Edmonds, T. M. McIntire, S. C. Milton, et al. 2004. Permeabilization of lipid bilayers is a common conformation-dependent activity of soluble amyloid oligomers in protein misfolding diseases. *J. Biol. Chem.* 279:46363–46366.
25. Qi, W. Z. A., D. Patel, S. Lee, J. L. Harrington, L. M. Zhao, et al. 2008. Simultaneous monitoring of peptide aggregate distributions, structure, and kinetics using amide hydrogen exchange: application to Abeta (1-40) fibrillogenesis. *Biotechnol. Bioeng*. 100:1214–1227.
26. Kheterpal, I., M. Chen, K. D. Cook, and R. Wetzel. 2006. Structural differences in A beta amyloid protofibrils and fibrils mapped by hydrogen exchange—mass spectrometry with on-line proteolytic fragmentation. *J. Mol. Biol.* 361:785–795.
27. Kheterpal, I., R. Wetzel, and K. D. Cook. 2003. Enhanced correction methods for hydrogen exchange-mass spectrometric studies of amyloid fibrils. *Protein Sci.* 12:635–643.
28. Klunk, W. E., R. F. Jacob, and R. P. Mason. 1999. Quantifying amyloid beta-peptide (A beta) aggregation using the Congo red A beta (CR-A beta) spectrophotometric assay. *Anal. Biochem.* 266:66–76.
29. Wang, S. S. -S., S. A. Tobler, T. A. Good, and E. J. Fernandez. 2003. Hydrogen exchange—mass spectrometry analysis of beta-amyloid peptide structure. *Biochemistry*. 42:9507–9514.
30. Olofsson, A., M. Lindhagen-Persson, A. E. Sauer-Eriksson, and A. Ohman. 2007. Amide solvent protection analysis demonstrates that amyloid-beta(1-40) and amyloid-beta(1-42) form different fibrillar structures under identical conditions. *Biochem. J*. 404:63–70.
31. Petkova, A. T., Y. Ishii, J. J. Balbach, O. N. Antzutkin, R. D. Leapman, et al. 2002. A structural model for Alzheimer's beta-amyloid fibrils based on experimental constraints from solid state NMR. *Proc. Natl. Acad. Sci. USA*. 99:16742–16747.
32. Williams, A. D., E. Portelius, I. Kheterpal, J. -t. Guo, K. D. Cook, et al. 2004. Mapping Aβ amyloid fibril secondary structure using scanning proline mutagenesis. *J. Mol. Biol.* 335:833–842.
33. Reference deleted in proof.
34. Walsh, D. M., D. M. Hartley, Y. Kusumoto, Y. Fezoui, M. M. Condron, et al. 1999. Amyloid beta-protein fibrillogenesis—structure and

biological activity of protofibrillar intermediates. *J. Biol. Chem.* 274:25945–25952.

35. Kheterpal, I., S. Zhou, K. D. Cook, and R. Wetzel. 2000. Aβ amyloid fibrils possess a core structure highly resistant to hydrogen exchange. *Proc. Natl. Acad. Sci. USA.* 97:13597–13601.
36. Williams, A. D., M. Sega, M. Chen, I. Kheterpal, M. Geva, et al. 2005. Structural properties of Aβ protofibrils stabilized by a small molecule. *Proc. Natl. Acad. Sci. USA.* 102:7115–7120.
37. Rochet, J. C., and P. T. Lansbury. 2000. Amyloid fibrillogenesis: themes and variations. *Curr. Opin. Struct. Biol.* 10:60–68.
38. Murphy, R. M. 2007. Kinetics of amyloid formation and membrane interaction with amyloidogenic proteins. *Biochim. Biophys. Acta.* 1768:1923–1934.
39. Kim, J. R., and R. M. Murphy. 2004. Mechanism of accelerated assembly of beta-amyloid filaments into fibrils by KLVFFK6. *Biophys. J.* 86: 3194–3203.
40. Wood, S. J., R. Wetzel, J. D. Martin, and M. R. Hurle. 1995. Prolines and amyloidogenicity in fragments of the Alzheimer's peptide beta/a4. *Biochemistry.* 34:724–730.
41. Maji, S. K., J. J. Amsden, K. J. Rothschild, M. M. Condron, and D. B. Teplow. 2005. Conformational dynamics of amyloid beta-protein assembly probed using intrinsic fluorescence. *Biochemistry.* 44:13365–13376.
42. Lazo, N. D., M. A. Grant, M. C. Condron, A. C. Rigby, and D. B. Teplow. 2005. On the nucleation of amyloid beta-protein monomer folding. *Protein Sci.* 14:1581–1596.
43. Borreguero, J. M., B. Urbanc, N. D. Lazo, S. V. Buldyrev, D. B. Teplow, et al. 2005. Folding events in the 21-30 region of amyloid-beta-protein (A beta) studied in silico. *Proc. Natl. Acad. Sci. USA.* 102:6015–6020.
44. Cruz, L., B. Urbanc, J. M. Borreguero, N. D. Lazo, D. B. Teplow, et al. 2005. Solvent and mutation effects on the nucleation of amyloid beta-protein folding. *Proc. Natl. Acad. Sci. USA.* 102:18258–18263.
45. Chimon, S., and Y. Ishii. 2005. Capturing intermediate structures of Alzheimer's β-amyloid, Aβ(1-40), by solid-state NMR spectroscopy. *J. Am. Chem. Soc.* 127:13472–13473.
46. Jang, S., and S. Shin. 2008. Computational study on the structural diversity of amyloid Beta Peptide (abeta(10-35)) oligomers. *J. Phys. Chem. B.* 112:3479–3484.
47. Nguyen, P. H., M. S. Li, G. Stock, J. E. Straub, and D. Thirumalai. 2007. Monomer adds to preformed structured oligomers of Abeta-peptides by a two-stage dock-lock mechanism. *Proc. Natl. Acad. Sci. USA.* 104:111–116.
48. Cheon, M., I. Chang, S. Mohanty, L. M. Luheshi, C. M. Dobson, et al. 2007. Structural reorganization and potential toxicity of oligomeric species formed during the assembly of amyloid fibrils. *PLoS Comput. Biol.* 3:1727–1738.
49. Kheterpal, I., A. Williams, C. Murphy, B. Bledsoe, and R. Wetzel. 2001. Structural features of the Abeta amyloid fibril elucidated by limited proteolysis. *Biochemistry.* 40:11757–11767.
50. Shivaprasad, S., and R. Wetzel. 2006. Scanning cysteine mutagenesis analysis of A beta-(1-40) amyloid fibrils. *J. Biol. Chem.* 281:993–1000.
51. Reference deleted in proof.
52. Zheng, J., H. Jang, B. Ma, and R. Nussinov. 2008. Annular structures as intermediates in fibril formation of Alzheimer A beta(17-42). *J. Phys. Chem. B.* 112:6856–6865.
53. Garzon-Rodriguez, W., A. Vega, M. Sepulveda-Becerra, S. Milton, D. A. Johnson, et al. 2000. A conformation change in the carboxyl terminus of Alzheimer's A beta(1-40) accompanies the transition from dimer to fibril as revealed by fluorescence quenching analysis. *J. Biol. Chem.* 275:22645–22649.
54. Simmons, L. K., P. C. May, K. J. Tomaselli, R. E. Rydel, K. S. Fuson, et al. 1994. Secondary structure of amyloid beta-peptide correlates with neurotoxic activity in-vitro. *Mol. Pharmacol.* 45:373–379.
55. Hertel, C., E. Terzi, N. Hauser, R. Jakob-Rotne, J. Seelig, et al. 1997. Inhibition of the electrostatic interaction between beta-amyloid peptide and membranes prevents beta-amyloid-induced toxicity. *Proc. Natl. Acad. Sci. USA.* 94:9412–9416.
56. Curtain, C. C., F. Ali, I. Volitakis, R. A. Cherny, R. S. Norton, et al. 2001. Alzheimer's disease amyloid-beta binds copper and zinc to generate an allosterically ordered membrane-penetrating structure containing superoxide dismutase-like subunits. *J. Biol. Chem.* 276:20466–20473.